

## Toward the validation of a newly developed CFD code: the case of a jet in cross flow

**Luís Fernando Figueira da Silva, Fernando Oliveira de Andrade**

Pontifícia Universidade Católica do Rio de Janeiro, Mechanical Engineering Department, Rua Marquês de São Vicente, 225  
22453-900 Rio de Janeiro/RJ Brazil  
{luisfer, fandrade}@mec.puc-rio.br

**Sandro Barros Ferreira**

Pontifícia Universidade Católica do Rio de Janeiro, Institute of Energy, Rua Marquês de São Vicente, 225  
22453-900 Rio de Janeiro/RJ Brazil  
sandro@ituc.puc-rio.br

**Abstract.** During the past few years a computational fluid dynamics computer code specifically tailored for compressible aerodynamical application has been developed by a group of Brazilian enterprises and universities. This code solves the transport equations of mass momentum and energy for both laminar or turbulent flows on general unstructured meshes. Several turbulence models are available. The governing equations are discretized by a finite volume technique, and different central and upwind schemes may be used for computing the fluxes. Temporal discretization may be performed either by explicit or implicit schemes, multigrid convergence acceleration is available. This work describes part of the code validation effort performed. A high speed jet in cross flow configuration, for which experimental data is available, is considered. The results obtained with the different turbulence models, spatial discretization schemes are compared to the experimental data and to computational results obtained with a commercial computer code. These comparisons show that the choices of the turbulence model and of the spatial discretization scheme exert a strong influence on the computed results.

**Keywords.** Jets, computational fluid dynamics, numerical study, code validation.

### 1. Introduction

Computational Fluid Dynamics (CFD) is a technique now integrated on the design phase of new aircraft. Besides the airframe itself, several subsystems of the aircraft rely on the flow of gases or liquids to perform according to the desired specifications. Among such subsystems lie the anti-icing, air conditioning and the engine. As a consequence, before it can be considered apt to using throughout the design process of the whole aircraft, any CFD tool should be thoroughly verified, and validated in circumstances representative of the functioning of these different systems. In particular, among the situations in which CFD tools are beginning to provide for innovative insights, is the operation of the thrust reversers during aircraft landing (Gatlin and Quinto, 1988, Strash, 1997, Trapp and Oliveira, 2003) and auxiliary air inlets (Pérez et al, 2006).

The present paper is related to the development of new computational tool specifically aimed at the prediction of flowfields characteristic of the aeronautical industry. This tool, which is the outcome of a partnership developed between Brazilian universities, research centers and enterprises, is tailored for the solution of compressible, turbulent, flowfields. The jets which are issued from the thrust reverser during landing are one of such flowfields of interest, and its prediction is the main motivation behind the computational results which will be presented here. However, the sheer complexity involved, where compressibility, turbulence, unsteady effects and tridimensional effects are interwoven (Andrade et al., 2006), precludes the direct use of such a configuration in code validation. Therefore, a representative situation of the thrust reverser configuration should be used in which the main physical characteristics are retained at the expense of pure geometrical complexity. In this work we have chosen the circular jet in a cross flow to represent the main flow characteristics found during thrust reverser operation.

This configuration has been calculated using the newly developed CFDk and Fluent CFD codes. The former code was under still under development, having few operational time and spatial discretization methods and turbulence models. The numerical results obtained using different turbulence models and spatial discretization options are compared to experimental data available (Margason, 1968, Schetz, 1980). A good agreement is shown to exist between the results obtained with both computer codes and the mean jet path. However, the overall jet shape and the jet breakdown patterns present some discrepancies. Before analyzing these results, a brief presentation is made of the models and the boundary conditions used.

### 2. Mathematical Modeling

The evolution of flowfields of interest is governed by the transport equations of mass, momentum and energy, i.e., the Navier-Stokes equations. Since the direct numerical simulation of the configuration studied is still beyond limits of

the available computational power, Reynolds averaging is used upon these transport equations. As these flow configurations involve variable density, the value of this property and of the pressure are decomposed as Reynolds (time) averages plus a fluctuation, whereas the remaining properties are treated by density-weighted (Favre) averaging. As a consequence, unclosed Reynolds stresses appear, representing correlations between the velocity fluctuations, which should be modeled. In this work four different models are used to express these unclosed terms: the Spalart-Allmaras (1992), the Shear Stress Transport (Menter, 1993), the realizable  $k-\epsilon$  (Shih et al., 1995) and the Reynolds Stress Model (Hanjalic and Launder, 1972). It is not the purpose of this paper to detail the models employed, which are supposed to have been implemented in their classical form by the code developers. Note that the source code was not open to us at the time this work was developed. The interested reader should consult the corresponding references if the aim is to gain insight on these models. However, one should note that the Spalart-Allmaras is a one-equation modified eddy viscosity transport model which was specifically developed for aerodynamic applications. The realizable  $k-\epsilon$  model is a recent extension on the classical  $k-\epsilon$  model, which uses the Boussinesq hypothesis to link the unclosed Reynolds stresses to the deformation tensor through an eddy viscosity. Lastly, the Reynolds Stress Model (RSM) solves six model equations for the Reynolds stresses, supplemented by an equation for the turbulence dissipation rate,  $\epsilon$ , and thus is not an eddy viscosity model. This model is, in principle, able to account for the production of turbulence by vorticity. It is, thus, expected that the RSM model presents the best results among the models used.

The computer codes used in this study employ different schemes to discretize the governing equations. On the one hand this is detrimental to the validation effort, since algorithm-specific issues could prevent useful conclusions to be drawn. On the other hand, if a good agreement is observed between the computed results, it could be likely that both codes correctly implement the equations.

The newly developed code, CFDk, is an edge-based, unstructured, finite volume code. Among several spatial discretization schemes available, this work uses Jameson's second order central differences and Roe's first order flux difference splitting schemes. These models were chosen since, at the time this work was performed, those were the models for which the multi-grid convergence acceleration technique was functional. The time integration technique used is a five-step Runge-Kutta scheme with second order accuracy, which was the only functional time-stepping scheme, although several others were under development. Cell based agglomeration multigrid convergence acceleration technique is used. The results obtained in this work considered three grid levels, with three interactions on the coarsest level. This code is based on previously tested algorithms (Bigarella et al., 2004, 2005), and further details can be obtained on these references.

Fluent is a general purpose commercial CFD code (Anon., 2006), which uses a pressure-based algorithm to solve the governing equations. In this work a steady state, implicit coupled solver was used. The interpolation scheme used for the convection term is the First-Order Upwind Scheme. The algorithm applied for the pressure-velocity coupling is SIMPLE.

### 3. Jet in Cross Flow Model

#### 3.1 Geometrical Configuration and Computational Mesh

The configuration analyzed is based on an experimental study, which consists of a 25.4 mm diameter jet situated next to the leading edge of a flat plate, directing the flow at a perpendicular angle into a subsonic freestream (Margason, 1968). Figure 1 shows the side and top view of the model configuration. The computed geometry consists of a rectangle, with a length of 30.5 times the jet diameter; a width of 24 times the jet diameter and a height of 20 times the jet diameter. These dimensions were chosen based on the actual wind tunnel cross section.

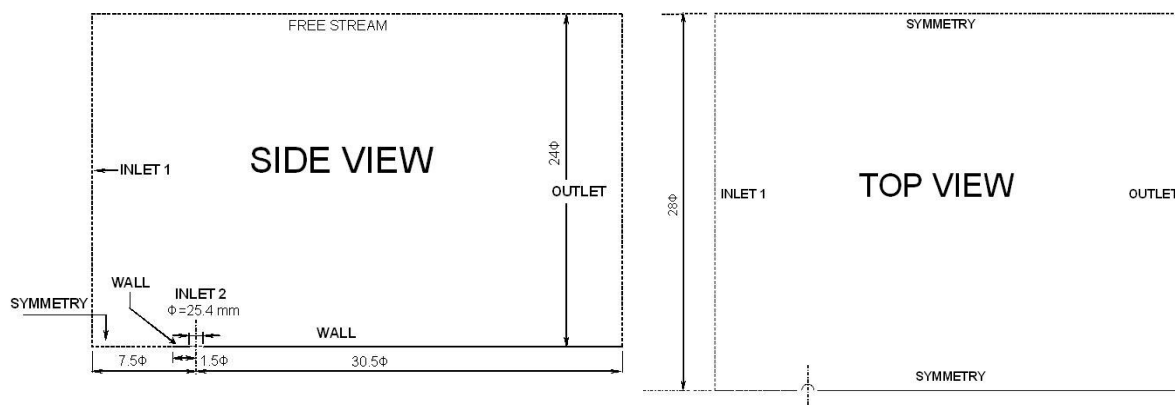


Figure 1. Side and top views of the CFDk jet in cross flow model configuration.

Figure 2 shows a perspective view of the computational mesh, which possesses approximately 400,000 elements. Results obtained with a mesh containing roughly 800,000 elements did not present significant discrepancies with respect to the coarse mesh results. Even if a detailed assessment of mesh convergence has not been attempted yet, the present mesh is considered sufficient for validation purposes. In figure 2 it can also be seen that the flow enters the INLET 1 face along the x-direction. The jet flow enters the domain at the INLET 2 and interacts with the freestream flow. The flow leaves the domain through the OUTLET face. Since no attempt was made to resolve the boundary layer which develops along the tunnel walls, symmetry is imposed on the lateral sides and on the top side of the computational domain. The bottom side is considered to be a smooth adiabatic wall. The use of symmetry conditions imply that only half of the circular jet is actually computed.

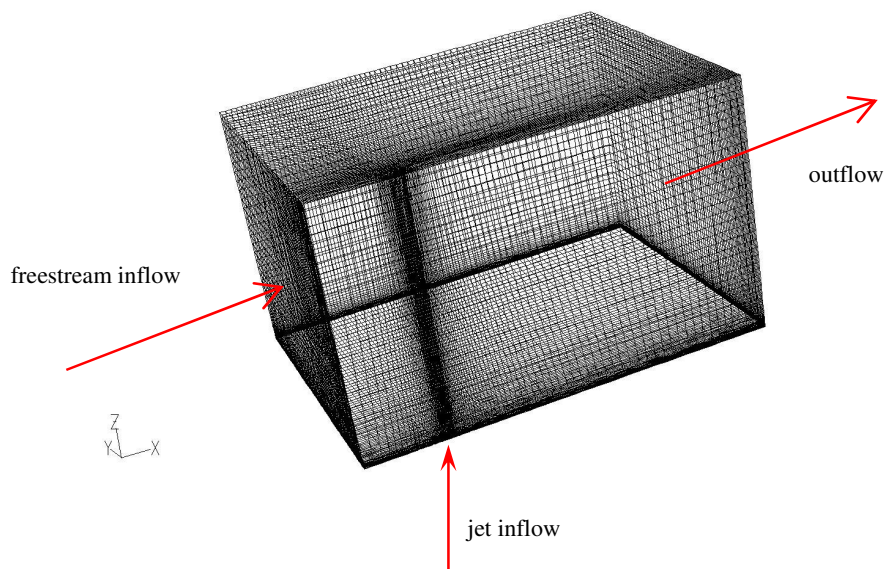


Figure 2. Perspective view of the mesh generated for the jet in cross flow application.

### 3.2 Boundary and Initial Conditions

The top, the sides and the symmetry plane upstream of the flat plate were assumed, for the sake of simplicity, as symmetry boundaries. The wind tunnel wall is an adiabatic no-slip stationary surface. The outflow was considered as a pressure outlet with a prescribed value of 101325 Pa. The wind tunnel inlet was considered to be a pressure inlet and corresponds to the x-axis oriented freestream entrance, where a total pressure of 103159 Pa, a static pressure of 101325 Pa, and a total temperature of 300 K were prescribed, resulting in a velocity of 67.5 m/s. The jet inlet is a z-axis oriented pressure inlet, and correspond to the jet entrance. A total pressure of 161005 Pa, a static pressure of 101325 Pa, and a total temperature of 300 K were prescribed, resulting in a jet velocity of 277.7 m/s.

The computations were initialized with the wind tunnel farfield conditions, using the data from the main air inlet.

### 4. Results and Discussion

This section presents the results of the jet in cross flow simulations obtained with Fluent for four different turbulence models: Spalart-Allmaras, Realizable  $k-\epsilon$ , SST and Reynolds Stress Model. The results of CFDk using the Spalart-Allmaras model, with First Order Roe and Jameson discretization methods are also shown. Table 1 summarizes the parameters of the simulations performed with the Fluent and CFDk packages.

The numerical results are compared with experimental data available (Margason, 1968, Schetz, 1980). The comparisons are performed in terms of the path of the jet into the subsonic freestream, and in terms of the cross sectional pressure contours for five planes normal to the jet.

Table 1. Configuration of the simulations with Fluent and CFDk.

CASE	Turbulence Model	Spatial Discretization	CFD Package
JSAR	Spalart Allmaras	1 order Roe	CFDk
JSAJ	Spalart Allmaras	Jameson	CFDk
JSAF	Spalart Allmaras	1 order upwind	Fluent
JKER	k-ε realizable	1 order upwind	Fluent
JSST	SST	1 order upwind	Fluent
JRSM	Reynolds Stress Model	1 order upwind	Fluent

#### 4.1 Jet Path Considerations

The experiment adopted for the CFDk validation used a water vapor injection flow visualization technique in order to provide for visible jet paths. In the experiments, the path of the jet perpendicular to the freestream was photographed through a range of effective velocity ratios from 0.10 to 0.83. Effective velocity  $V_e$  is defined as the square root of freestream dynamic pressure to the jet dynamic pressure

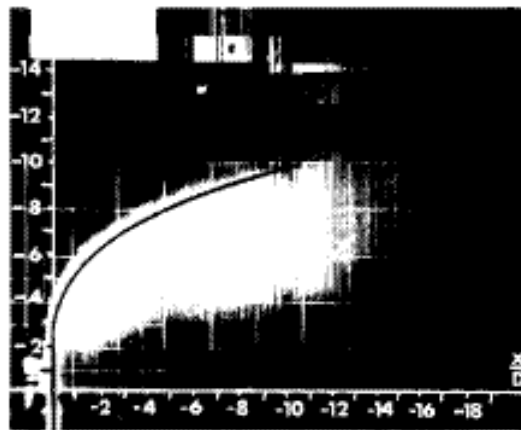
$$V_e = \sqrt{\frac{\rho_\infty V_\infty^2}{\rho_j V_j^2}} \quad (1)$$

An empirical equation of the center line of the jet was developed, compared and validated with previous investigations. The form of this equation describes the locus of maximum pressures in the jet wake,

$$\frac{x}{D} = k \left( \frac{z}{D} \right)^a V_e^b \quad (2)$$

where k, a and b are -0.25, 3, and 2 respectively, and D is the jet diameter. This equation is applicable up to a region of 10 to 12 diameters downstream from the jet exit.

Figure 3 shows a photograph superimposed with the empirical correlation of the jet path for a value of effective velocity  $V_e$  of 0.21, and a ratio of the jet dynamic pressure to the atmospheric pressure of 0.589. This particular experimental result is used here for validation purposes.



(a)  $V_e = 0.210$ ;  $q_j/p_a = 0.589$ .

Figure 3. Water vapor visualization of the jet in cross flow.

### 4.2 Convergence of the Solutions

Figure 4 shows the residuals for the jet in cross flow simulation using Fluent with the Spalart-Allmaras (JSAF case),  $k-\epsilon$  Realizable (JKER case), SST (JSST case) and Reynolds Stress (JRSM case) turbulence models, and using CFDk with the Spalart-Allmaras model, first order Roe (JSAJ case) and Jameson (JSAJ case) spatial discretization methods, respectively.

The case JSAF, which used the Spalart-Allmaras turbulence model, achieved stabilization of the residuals after 10,000 iterations, however with an important oscillation. The residuals ranged between  $10^{-3}$  for the y-velocity component to  $10^{-7}$  for the modified turbulent viscosity. The case using the  $k-\epsilon$  Realizable model achieved convergence after 5,000 iterations. The residuals ranged between  $10^{-5}$  for the y-velocity component to around  $10^{-7}$  for the turbulent kinetic energy. The case using the SST model achieved convergence after 6,000 iterations. The residuals ranged between  $10^{-3}$  for the y-velocity component to around  $10^{-5}$  for the turbulence dissipation rate. Note that the case using the Reynolds Stress model achieved convergence after 6,000 iterations, but only after the coupled solver was replaced by the segregated one at the iteration 3,000. This led all the residuals to the range of  $10^{-7}$ , achieving a stall of convergence.

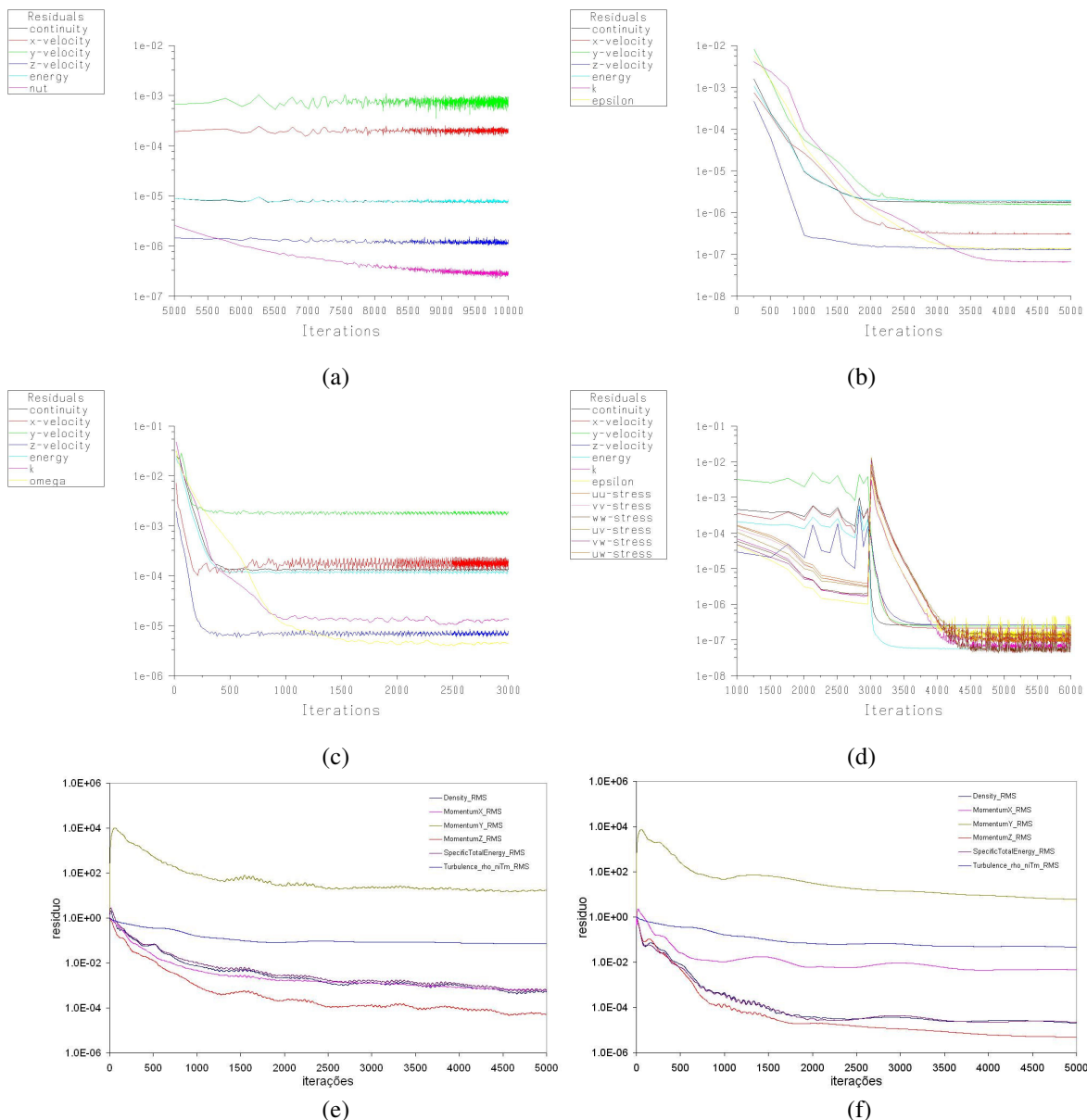


Figure 4. Evolution of the RMS values of the residuals, cases: (a) JSAF, (b) JKER, (c) JSST, (d) JRSM, (e) JSAJ, and (f) JSAR.

For the CFDk case JSAJ, the normalized residuals became stable after 5,000 iterations. The normalized residuals for the x and z components of momentum, energy, and continuity stabilized around a value of  $10^{-4}$ . The normalized residuals for the y component of momentum became stable at  $10^2$  and the modified turbulent viscosity achieved a

steady state around  $10^1$ . Note that, despite these high values, which are due to the normalization, there is at least a two order of magnitude decrease in the residuals for each property, with the exception of the modified turbulent viscosity.

For the JSAR case, the normalized residuals also became stable after 5,000 iterations. The normalized residuals for the x component of momentum, energy, and continuity stabilized around a value of  $10^{-5}$ . The normalized residuals for the z component of momentum stabilized around  $10^{-2}$ . The normalized residuals for the y component of momentum became stable at  $10^2$  and the modified turbulent viscosity achieved a steady state around  $10^1$ .

### 4.3 Jet Path Comparisons

The jet comparisons are performed based on a high momentum experimental configuration (Margason, 1968), which corresponds to the greater ratio of the jet velocity to the freestream velocity. The calculated effective velocity is equal to 0.21 and the ratio of the jet dynamic pressure to the atmospheric pressure is 0.589.

Figures 5 and 6 show the distributions of modulus and of the x-component of momentum, respectively. The results are shown at the jet longitudinal symmetry plane for the cases using Fluent with the Spalart Allmaras,  $k-\varepsilon$  Realizable, SST and Reynolds Stress turbulence model, and using CFDk with Spalart Allmaras model with first order Roe and Jameson discretization methods. The obtained numerical results are compared to the experimental jet path available (Margason, 1968). Figure 7 shows the velocity vector distribution at the jet longitudinal symmetry plane for these cases.

Initially, it is important to note that all simulation results exhibited a good agreement with the experimental jet path, with small discrepancies related to the choice of turbulence model. Analyzing the results obtained with Fluent using the four different turbulence models, it can be noted that the Spalart-Allmaras and the  $k-\varepsilon$  Realizable models produced quite similar results. The results of the SST model differed from the former two, presenting a larger spreading around the jet centerline and a small discrepancy concentrated on the region of the jet exit. The most important differences were presented by the Reynolds Stress model, which led to a considerably different momentum distribution from the three other cases, mainly on the region downstream from the jet, where a reverse flow region is more evident. Note that the shape of the reverse flow region is more elongated in this case. According to Ibrahim and Gutmark (2006) the reverse flow region is formed as the cross flow travels around the periphery of the jet column and gets pulled back into the origin region of the jet. This occurs due to the influence of the adverse pressure gradient which results, leeward of the jet, from the blockage effect of the jet to the oncoming cross flow. The reverse flow acts to support the jet on the leeward side by inducing local upward lifting force to lift-off the jet from the wall. The strength of the reverse flow region is dependent on the extent of blockage the jet poses to the freestream. This translates into the rate of deceleration of the freestream as it travels around the jet as well as the magnitude of the adverse pressure gradient developed. In such a flow configuration, where vorticity may lead to turbulence generation, the RSM is presumably the most accurate model.

Concerning the CFDk results, it can be seen that the results of the JSAJ case are similar to those of the JRSM case, which is rather surprising and could not be expected. An explanation for the presence of a secondary plume in the JSAJ case is lacking. The use of Roe first order spatial discretization together with the Spalart-Allmaras model led to results which are quite similar to those obtained with Fluent (JSAF). However, the jet plumes computed with CFDk seem to diffuse less than those obtained with Fluent.

The development of the boundary layer along the wall is similar for the Fluent computations using the Spalart-Allmaras, realizable  $k-\varepsilon$  and SST models, whereas the CFDk computed boundary layer closely resembles the one computed with the RSM, which presents a smaller thickness. This may be attributed to lower levels of artificial dissipation added to the spatial discretization algorithms present at the CFDk, but require further analysis for confirmation. Since no measurements of the boundary layer are available, it is impossible to determine which result better corresponds to the experiments in such a tri-dimensional flowfield.

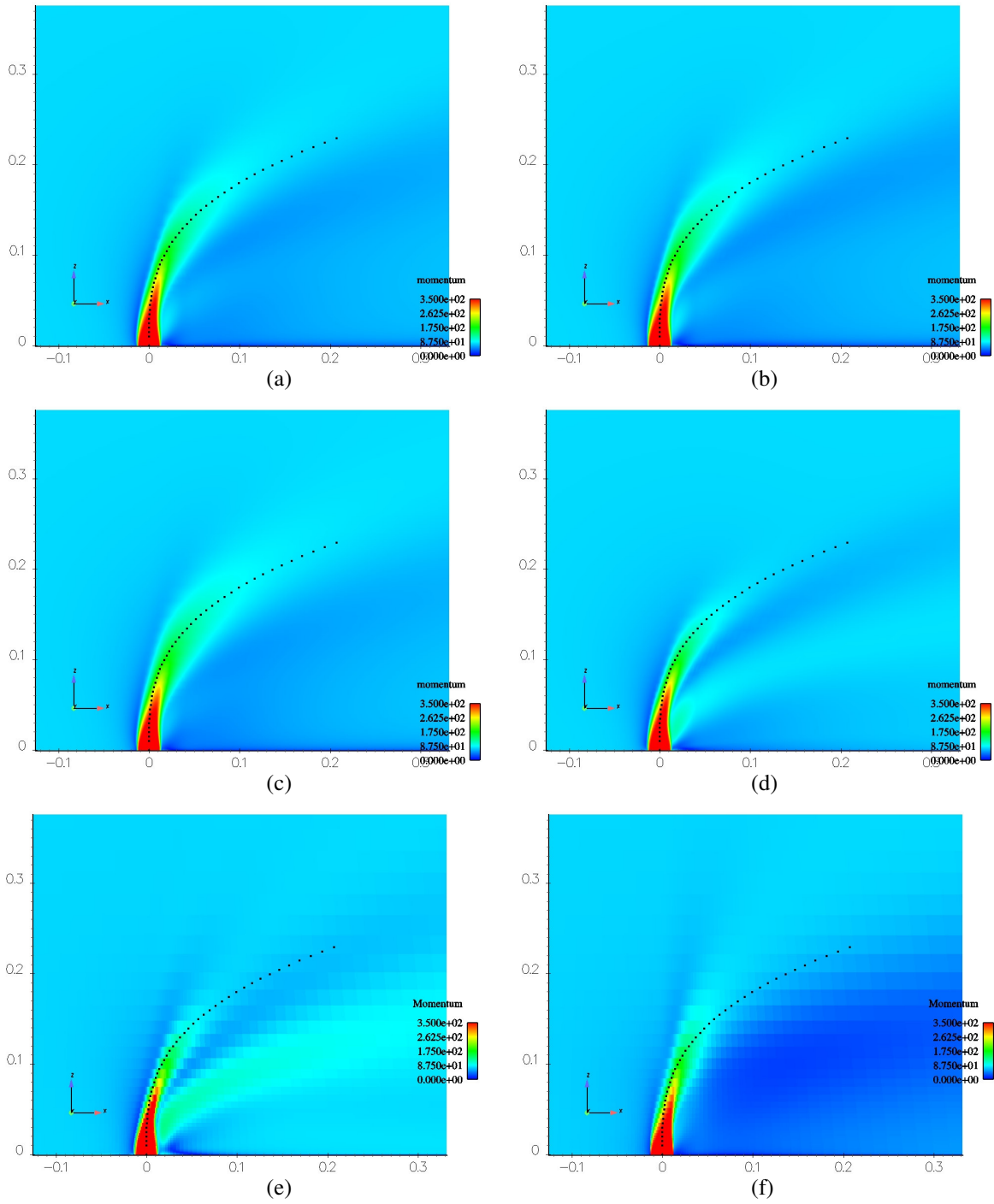


Figure 5. Comparison of the jet momentum distribution to the empirical jet path (dimensions in m); cases: (a) JSAF, (b) JKER, (c) JSST, (d) JRSM, (e) JSAJ, and (f) JSAR.

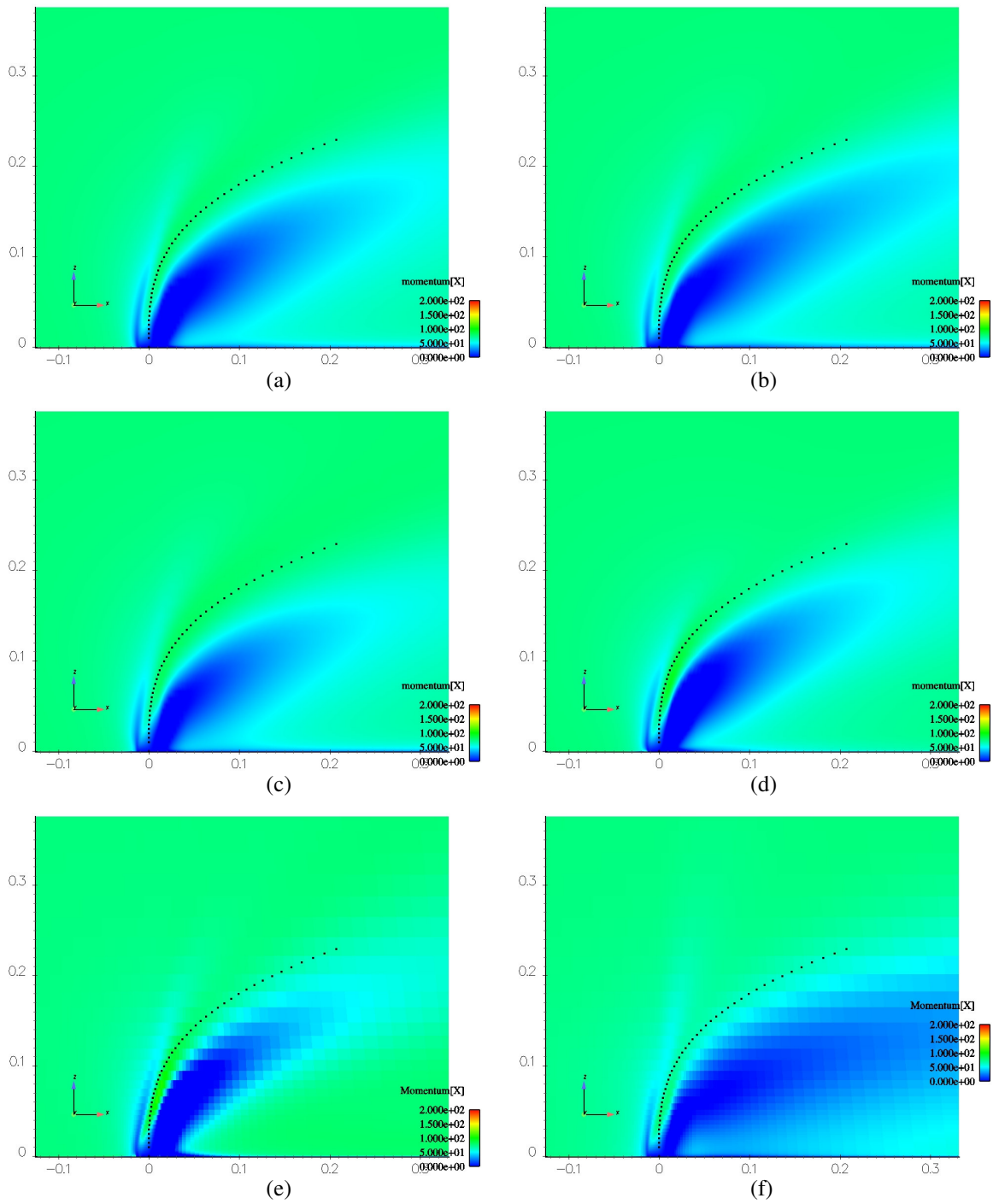


Figure 6. Comparison of the jet x-momentum distribution to the empirical jet path (dimensions in m); (a) JSAF case, (b) JKER case, (c) JSST case, (d) JRSM case, (e) JSAJ case, and (f) JSAR case.

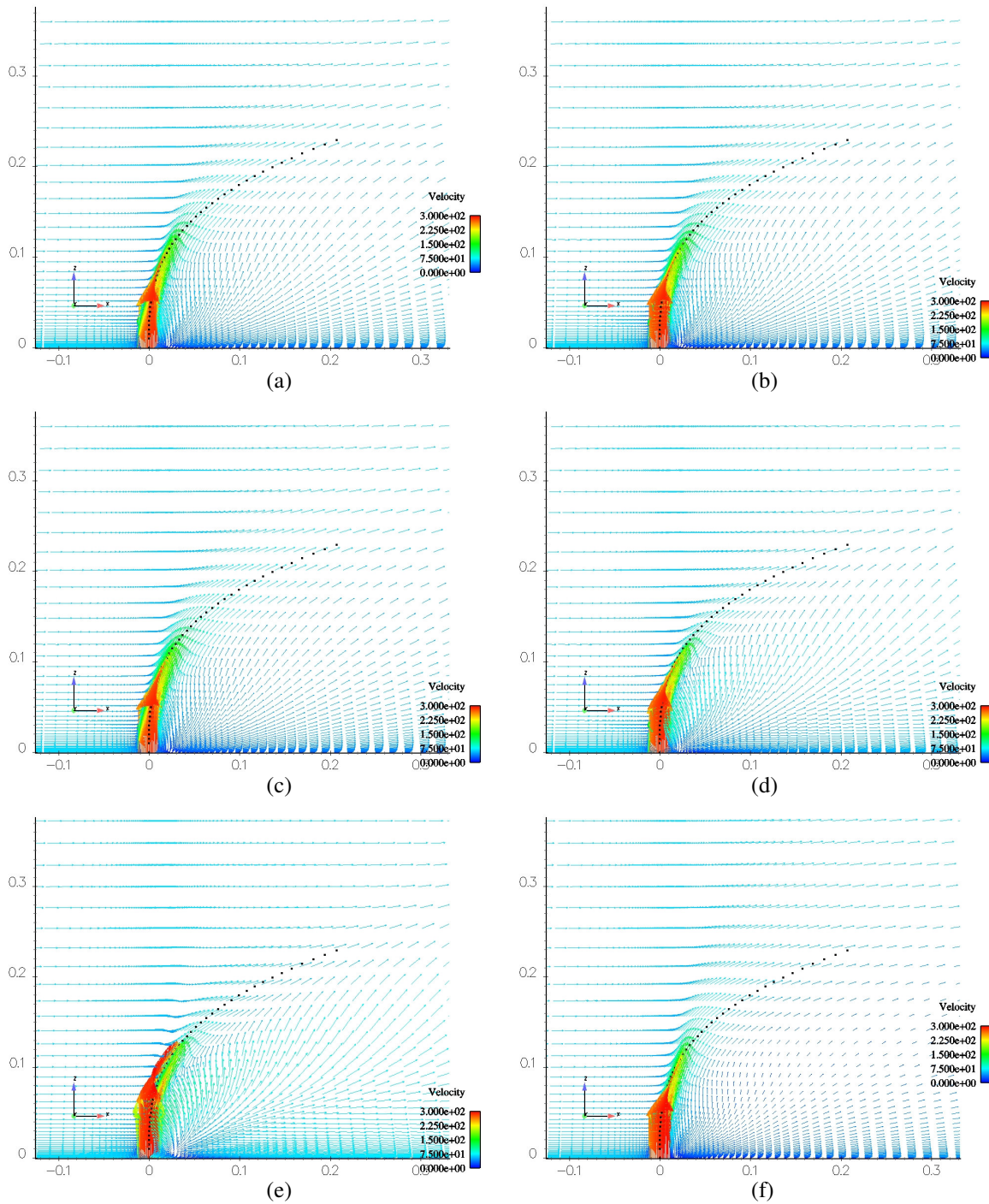


Figure 7. Comparison of the velocity vector distribution to the empirical jet path (dimensions in m); cases: (a) JSAF, (b) JKER, (c) JSST, (d) JRSM, (e) JSAJ, and (f) JSAR.

#### 4.4 Pressure Contours Comparisons

The comparisons are performed based on the pressure distribution for five planes normal to the jet at different heights from the wall (Schetz, 1980). The overall structure of the flow for a case with 90 degree injection can be seen in Figure 8, where are shown the pressure contours in cross sections which are perpendicular to the initial orientation of the jet. The “bean-shaped” nature of the jet as it is deflected and distorted by the cross stream is particularly visible. Another characteristic is a stretch of the shape as the jet develops along the cross-sections. It is expected that the calculated momentum of the jets at the five normal planes follow the same bean-shaped behavior observed in the experiments for the static pressure evolution.

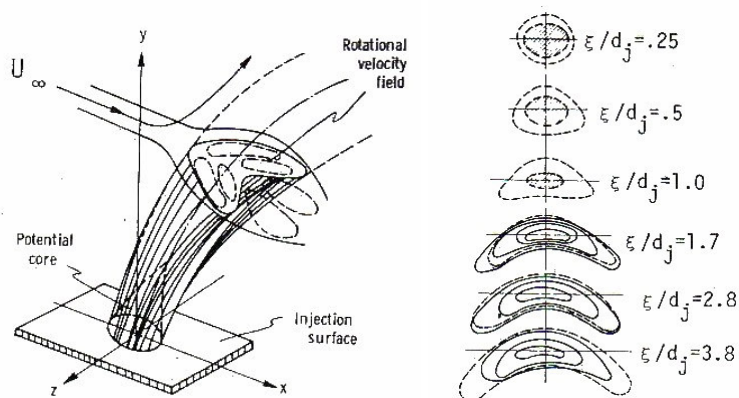
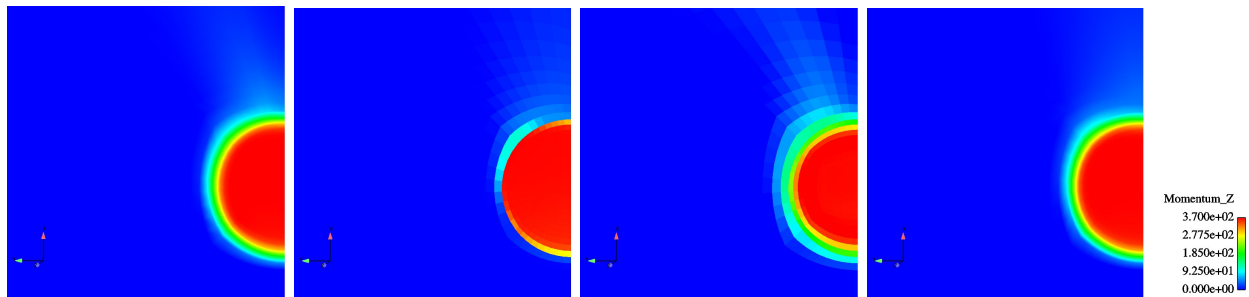


Figure 8. Cross-section pressure contours in a transverse jet; solid and dashed lines are constant of static pressure, and the shaded areas denote the potential core (Schetz, 1980).

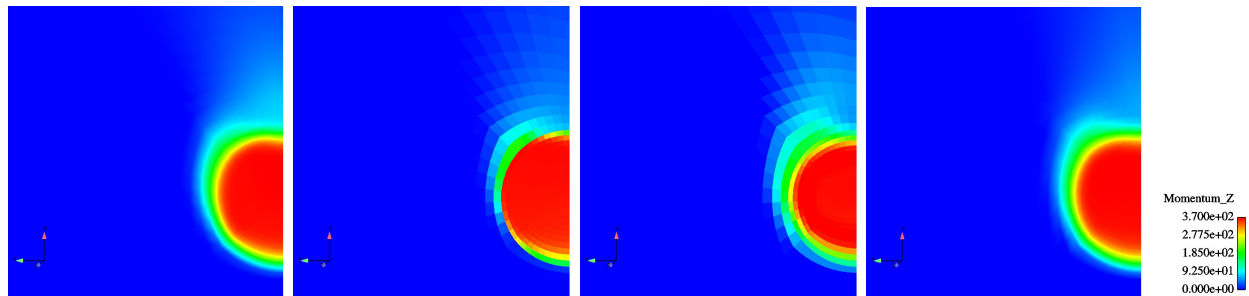
Figure 9 shows the contours of  $z$ -momentum for planes parallel to the wall located at 0.25, 0.50, 1.00, 1.70 and 2.80 diameters above the jet exit. In this figure, results obtained with Fluent using both the RSM and Spalart-Allmaras models and CFDk with the Spalart-Allmaras model and the two spatial discretizations considered. The results obtained with the RSM are clearly in good qualitative agreement when compared with the pressure contours of Fig. 8. The progressive distortion and breakdown of the calculated jet closely follows the experimental behavior, and the computed aspect ratio of the bean-shaped jet resembles that of the experiments.

The secondary jet plume is evident in the results obtained with the RSM. This plume can also be observed in the results obtained with the CFDk code using the Spalart-Allmaras model together with the Jameson spatial discretization method. The results of this case, JSAJ, also exhibit a much larger jet breakdown, which is evident by the large aspect ratio of the momentum contours. The results obtained with the Spalart-Allmaras model using Fluent and the CFDk with first order Roe spatial discretization are quite similar. The development and breakdown of the jet are practically identical, and the final aspect ratio of the bean-shaped jet smaller than those observed in the cases JRSM and JSAJ. The fact that both Fluent and CFDk first order schemes yield similar results indicates that the Spalart-Allmaras implementation of the CFDk is correct at least when the Roe scheme is used.

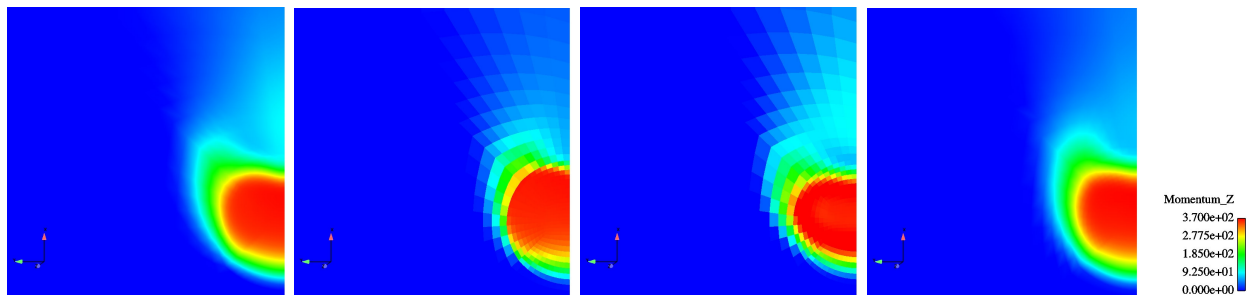
Furthermore, the results shown in Fig. 9 can be understood by recalling that the Jameson spatial discretization is a centered second order scheme, and thus *a priori* less dissipative than either the Fluent first order upwind scheme or the first order Roe scheme implemented in the CFDk. Thus the more elongated distortion of the jet in the JSAJ case when compared to the JSAR one, and also the ability of the computation with the Jameson method to capture the secondary plume predicted in the second-order RSM. This plume is practically absent from the first order computations, possibly due to the dissipative nature of the discretization. Thus, it is expected that the Jameson second-order discretization is correctly implemented in the CFDk.



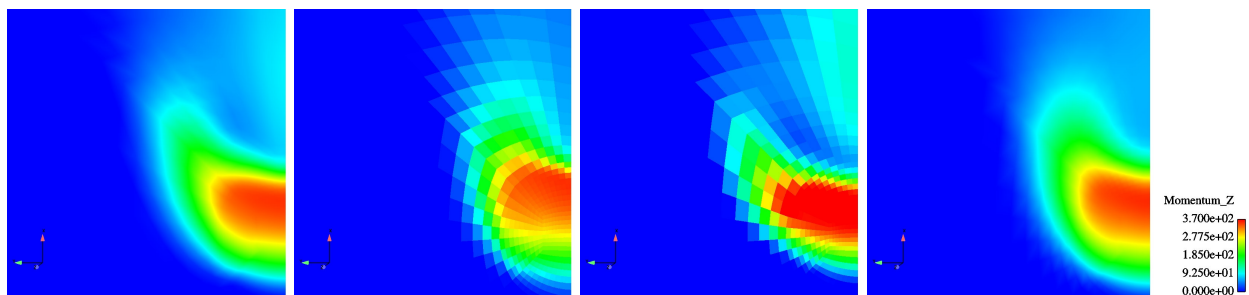
(a) horizontal plane located 0.25 diameters above the jet exit,



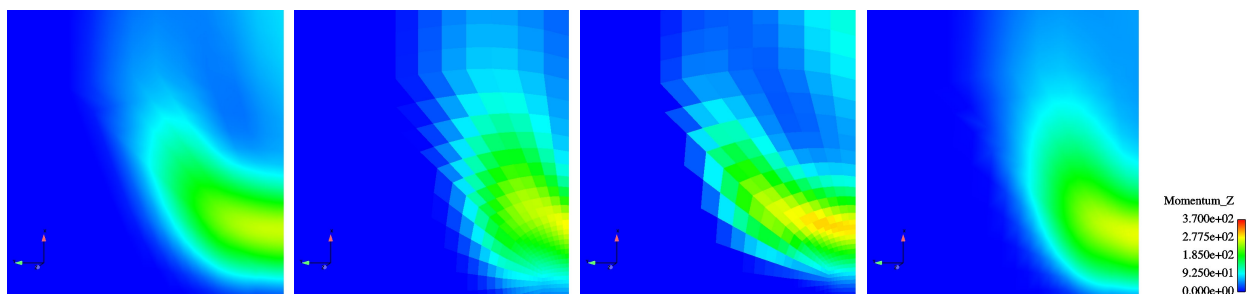
(b) horizontal plane located 0.50 diameters above the jet exit,



(c) horizontal plane located 1.00 diameters above the jet exit,



(d) horizontal plane located 1.70 diameters above the jet exit,



(e) horizontal plane located 2.8 diameters above the jet exit,

Figure 9. Contours of z-momentum for planes parallel to the wall, located at different heights above the jet exit: from left to right, cases JRSM, JSAR, JSAJ and JSAF. The dimensions of all figures correspond to 60 mm in the longitudinal direction and 57 mm in the transversal direction of the jet.

## 5. Conclusions

The CFDk validation study was performed through the comparison of the CFDk results with Fluent results. Both numerical results were compared to the experimental data available in terms of the path of the jet into the subsonic freestream, and in terms of the cross sectional pressure contours for five planes normal to the jet. The CFDk results used for the comparisons were obtained using the Spalart-Allmaras turbulence models with first order Roe, and second order Jameson spatial discretization methods, respectively. The Fluent computations considered four different turbulence models, including a second-order Reynolds Stress Model.

The CFDk results showed good agreement with the experimental data in terms of the jet path, even though the overall structure of the flowfield was not entirely coincident with the Fluent results. The analysis of the jet breakdown in terms of the evolution of the momentum in planes perpendicular to the jet allowed confirming that the results obtained with Fluent and CFDk with the Spalart-Allmaras model using first order spatial discretizations are in very good agreement. Finally, the results obtained with the second order Jameson's spatial discretization method were shown to be less dissipative than those computed with the first order methods. The jet breakdown is more developed than in the first order computations and seem to closely follow the experimental results. However, validation can only be proven once the computed results are compared to detailed experimental data.

## 6. Acknowledgements

This work was performed with financial support from Embraer and Fapesp while the first author was on leave from *Laboratoire de Combustion et de Détonique, Centre National de la Recherche Scientifique*, France. Mr. Rodrigo Ferraz, from Engineering Simulation and Scientific Software, Ltda., was responsible for the mesh generation.

## 7. References

- Andrade, F. O., Ferreira, S. B., Figueira da Silva, L.F., Jesus, A. B. and Oliveira, G. L., 2006, "Study of the influence of aircraft geometry on the computed flowfield during thrust reverser operation," 24<sup>th</sup> AIAA Applied Aerodynamics Conference, AIAA Paper 2006-3673, San Francisco.
- Anonimous, 2006, "Fluent 6.0 User's Guide," Fluent 6.0 Documentation, Fluent Inc.
- Bigarella, E. D. V., Basso, E. and Azevedo, J. L. F., 2004, "Centered and Upwind Multigrid Turbulent Flow Simulations with Applications to Launch Vehicles," 22<sup>nd</sup> AIAA Applied Aerodynamics Conference and Exhibit, AIAA Paper 2004-5384, Providence.
- Bigarella, E. D. V., Basso, E. and Azevedo, J. L. F., 2005, "A Study of Convective Flux Computation Schemes for Aerodynamic Flows," 43<sup>rd</sup> AIAA Aerospace Sciences Meeting and Exhibit, AIAA Paper 2005-0633, Reno.
- Gatlin, G. M. and Quinto, P. F., 1988, "Thrust-reverser flow investigation on a twin-engine transport", NASA-TP-2856; L-16426; NAS 1.60:2856 , 19881201
- Hanjalic, K. and Launder, B. E., 1972, "A Reynolds stress model of turbulence and its application to thin shear flows", *Journal of Fluid Mechanics*, Vol. 52, pp. 609-638.
- Ibrahim, I. M. and Gutmark, E. J., 2006, "Dynamics of single and twin circular jets in cross flow", 44<sup>th</sup> AIAA Aerospace Science Meeting and Exhibit, AIAA Paper 2006-1281, Reno, USA.
- Margason, J. R., 1968, "The Path of a Jet Directed at Large Angles to a Subsonic Free Stream", NASA Technical Note TN D-4919
- Menter, F. R., 1993, "Zonal two-equation k- $\omega$  turbulence model for aerodynamic flows", AIAA Paper 1993-2906.
- Pérez, C. C., Figueira da Silva, L. F., Ferreira, S. B., Jesus, A. B. and Oliveira, G. L., 2006, "Numerical Study of the Performance Improvement of Submerged Air Intakes Using Vortex Generators," 25<sup>th</sup> Congress of International Council of Aeronautical Sciences, Hamburg, Germany.
- Schetz, J. A., 1980, "Injection and Mixing in Turbulent Flow", *Progress in Astronautics and Aeronautics*, Vol. 68. American Institute of Aeronautics and Astronautics.
- Shih, T.-H, Liou, W.W., Shabbir, A., Yang, A. and Zhu, J., 1995, "A new k- $\epsilon$  eddy viscosity model for high Reynolds number turbulent flows", *Computers and Fluids*, Vol. 24, No. 3, pp. 227-238.
- Spalart, P. R. and Allmaras, S. R., 1994, "A one-equation turbulence model for aerodynamic flows," *La Recherche Aérospatiale*, No. 1, pp. 5–21.
- Strash, D. J., Summa, J. M., Frank, J. H. and Standish, R., 2000, "Aerodynamic Analysis of an Installed Thrust Reverser", *Journal of Propulsion and Power*, Vol.16 No. 1, pp. 10-15.
- Trapp, L. G. and Oliveira G. L., 2003, "Aircraft Thrust Reverser Cascade Configuration: Evaluation Through CFD", 41<sup>st</sup> Aerospace Science Meeting & Exhibit, American Institute of Aeronautics and Astronautics.